2-D Flow and Temperature Measurements in a Multiphase Airlift Crystallizer

ARTICLE *in* INDUSTRIAL & ENGINEERING CHEMISTRY RESEARCH · AUGUST 2013

Impact Factor: 2.59 · DOI: 10.1021/ie4006723

I&EC research
Industrial & Engineering Chemistry Research

Article

pubs.acs.org/IECR

2-D Flow and Temperature Measurements in a Multiphase Airlift Crystallizer

Anamaria Soare,* Sergio A. Pérez Escobar, Andrzej I. Stankiewicz, Marcos Rodriguez Pascual, and Herman J. M. Kramer

Intensified Reaction and Separation Systems, Delft University of Technology, 2628 CA Delft, The Netherlands

ABSTRACT: A combined particle image velocimetry (PIV) and particle image thermometry (PIT) method was applied to visualize and measure simultaneously the 2-D velocity and temperature fields in a crystallizer. The 2-D supersaturation field can be also determined before nucleation or seeding takes place. The hydrodynamic behavior in an internal loop airlift crystallizer was studied for different air flow rates, sparger types, and crystal holdups to get insight in the optimal process conditions for this crystallizer, i.e. uniform temperatures and particle concentration. The 2-D velocity and temperature gradients showed that in a 2 L crystallizer the mixing is sufficient to ensure uniform supersaturation profiles at an overall superficial air velocity higher than 2.3 mm/s. Suspension tests showed that a superficial air velocity of 7 mm/s was sufficient to avoid settling of the crystals. This air flow rate assured the lifting of the solids from the bottom of the crystallizer for crystals with a mean size of 1.5 mm and holdups up to 10 wt %. Both the circulation velocity and the crystal holdup which could be totally suspended increased with the air flow rate. For the ammonium sulfate−water system, the crystal growth behavior, which is also influenced by the mixing, was theoretically studied. The growth of the crystals in an airlift crystallizer behaves comparable to that in a suspension stirred crystallizer, and no evidence for mass transfer limitation of the crystal growth was found.

1. INTRODUCTION

Crystallization from solution is an important separation technology which has the advantage that a high-purity solid product is obtained in a single processing step, at a relatively low level of energy consumption and mild process conditions. A variety of crystallizer designs is used for industrial crystallization processes.[1,2] An important aspect in the design of these crystallizers is to ensure sufficient mixing of the solute and a complete suspension of the crystals within the crystallizer to avoid supersaturation profiles. In most of the designs, impellers or pumps are used to achieve this. The major drawback of the use of impellers and pumps in crystallizers however is that their mechanical contacts with the crystal leads to attrition and breakage. The resulting secondary nucleation is difficult to control due to its coupling to the mixing of the suspension and leads to smaller mean sizes and broader crystal size distributions.[3,4] The airlift crystallizer is a promising alternative for the commonly used stirred crystallizer to avoid secondary nucleation by attrition.[5]

Airlift columns are encountered for applications in biotechnology[6] due to the low shear forces present in air-mixed devices which help to prevent damage to micro-organisms.[7,8] Despite the advantage of decreasing the shear forces on the crystals offered by gas lift devices, their acceptance in the crystallization field has been low. Haut et al.[9] developed a model to describe the precipitation of sodium bicarbonate in an industrial bubble column, which was partially equipped with an airlift. The measurements proved that the solid phase was perfectly mixed only in the zone where the airlift motion was created. Saberi et al.[10] showed experimental results from an industrial bubble column crystallizer which indicated that growth of crystals is size independent and agglomeration of crystals does not exist. Rigopoulos and Jones[11] developed a model for the precipitation of $CaCO_3$ in a bubble column, which included the nucleation, growth and agglomeration of crystals, mass transfer, reaction kinetics, and gas holdup. The authors concluded that the model gave qualitative comparison with the experimental CSD, but more fundamental research on the hydrodynamic environment is required to obtain quantitative agreement.

It has been shown in a previous study[5] that in an airlift crystallizer secondary nucleation generated by attrition and breakage can be minimized due to the absence of an impeller and that the final crystal size can be close to the ideal size, i.e. the size calculated under the assumption that only crystal growth occurs. Primary and secondary nucleation could be minimized during batch operation by the application of an optimized supersaturation profile minimizing at the same time the shear stress on the crystal, by manipulation of the air flow and the sparger design. However it also appeared that the hydrodynamic design of the crystallizer is not trivial and has a strong impact on the flow regime in the crystallizer, the mixing of the solution phase, the settling behavior of the crystals, and on the mass transfer from the solution to the crystal phase.[5]

The air flow rate, the sparger geometry, and the ratio between the cross sectional areas of the riser and down-comer are the most important factors which influence the hydrodynamics in the crystallizer. The easiest way to manipulate the hydrodynamics and therefore the liquid circulation velocity is by changing the air flow rate. The flow rate of pressurized air injected in the riser of the crystallizer has an influence on the

Received: March 1, 2013
Revised: July 15, 2013
Accepted: July 25, 2013
Published: July 25, 2013

size and shape of the bubbles, on the bubbles velocities, and on the gas hold-up. All these factors have a large influence on the solution circulation velocity and on the flow regime.

Three flow regimes may be distinguished in an airlift crystallizer:[7] regime I, characterized by the absence of gas entrainment in the down-comer; regime II, characterized by gas entrainment but no gas recirculation; and regime III, characterized by complete gas recirculation of the entrained bubbles.

Previous results[5] showed that for crystallization, regime I is preferred and that the liquid circulation velocity determines the performance of the crystallizer. However the required liquid circulation velocity in this type of crystallizer, to avoid settling of the larger crystals and preventing the mass transfer between the liquid and the solid phase, is not known. Because of the complexity of the multiphase flow in the airlift crystallizer, measurements of the flow conditions and the mixing are essential for the characterization of the hydrodynamic behavior and for a better understanding of the crystallizer's performance.

Conventional techniques to study the flow behavior, which use pitot tubes, venturi tubes, or rotameters, cannot be used in crystallizers because of the two (or three) phase character of the flow. An alternative is to use hot-wire anemometry, ultrasound, or laser Doppler velocimetry which are used to measure flow rate in pilot scale as well as large scale operating industrial system. These are point measurement methods which may provide very high resolution time histories of the velocity at a point. However, if a flow is not steady, precisely repeatable or periodic, then single point methods cannot be used to build up a 2-D velocity map in a point by point manner. 2-D methods are a relatively recent addition to the methods of flow measurement. Particle image velocimetry, or PIV, refers to a class of methods used in experimental fluid mechanics to determine instantaneous fields of the vector velocity by measuring the displacement of numerous fine particles that accurately follow the motion of the fluid.[12] The acquisition of velocity and temperature information can be done simultaneously with the use of thermo-sensitive liquid crystals. A combined PIV and PIT method, in which the liquid crystals are used in the PIV to trace the liquid flow and in the PIT measurement to monitor the local temperature, was used before to study convective flows within confined cavities and vortex flows. Ozawa et al.[13] were among the first to perform simultaneous temperature and velocity measurements within a fluid flow. They studied the natural convection in a parallelepiped cell by using a liquid-crystal tracer. Hiller et al.,[14,15] Dabiri et al.,[16] and Li[17] studied the effect of steady and oscillating heating and cooling of the side walls on mixing within a cubic cavity. Kowalewski[18,19] studied the freezing process of water in a differentially heated cubic cavity. Park et al.[20,21] investigated the wake of a heated cylinder using PIV and PIT.

The research presented in this paper has two main objectives: first to develop a method to visualize and measure the velocity, temperature, and initial supersaturation fields in real time throughout the vessel and second to apply this method to study the hydrodynamic conditions in an airlift crystallizer with respect to circulation velocity, mixing, and suspension capability. The results of the study are used to optimize operation conditions for minimum temperature and supersaturation gradients and complete suspension at different solid holdups.

The experimental setup involving a 2 L crystallizer and the method for simultaneously measuring velocity, temperature, and supersaturation profiles is described. The importance of the results for the design and operation of airlift crystallizer is discussed.

2. EXPERIMENTAL SETUP AND METHODS

2.1. Experimental Setup. To demonstrate the feasibility of the 2-D supersaturation measurements, experiments were conducted in a cylindrical glass jacketed vessel. The internal diameter and the height of the vessel are 124 and 210 mm, respectively. The model compound was ammonium sulfate in water.

To study the hydrodynamics in an airlift crystallizer experiments were performed in the same vessel, in which a riser and an air sparger were introduced. A schematic picture of the laboratory scale airlift crystallizer setup is presented in Figure 1. The diameter of the riser is 75 mm, the height is 170 mm, and it has 4 baffles on the exterior part. The baffles are vertically positioned, equally spaced, and have the same height as the riser and a width of 10 mm. The clearance between the bottom and the riser is 17 mm. The sparger is placed in the center of the vessel at the lower end of the riser. Two types of spargers are used (see Figure 2).

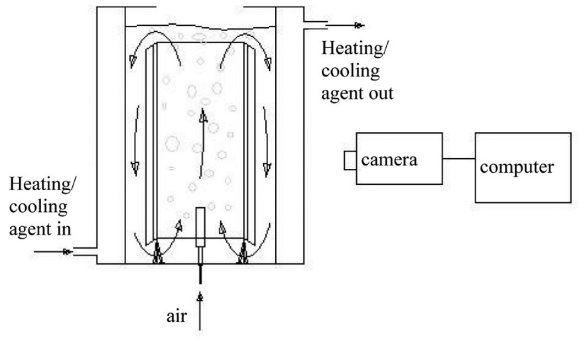

Figure 1. Schematic setup of the laboratory installation; an illuminator generating a sheet of light of 2−3 mm was positioned perpendicular to the camera.

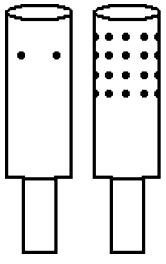

Figure 2. Geometry of the used spargers. The spargers are closed cylindrical pipes with 10 mm diameter, 30 mm height and with 4 or 32 holes of 1 mm diameter each.

A schematic picture of the two spargers is presented in Figure 2. The first sparger has 4 holes arranged uniformly on a circle around the circumference of the sparger pipe. The second sparger has 32 holes arranged uniformly on 4 circles around the circumference of the sparger pipe.

A high speed color digital camera (Mikrotron, EoSens, MC3011) was used to capture the photographic images to track

the liquid crystal particles added in the solution (Nematic LC Slurry, NSL40/R25C10W, LCR Hallcrest LTD). Two droplets of liquid crystals slurry were added to the solution with a final concentration of 20 volume ppm. The mean diameter of the microcapsules was 100 μm, small enough to be good flow tracers and large enough to scatter sufficient light for the imaging. The code R25C10W describes a thermochromic liquid crystal mixture with the start of the red color at 25 °C and a bandwidth of 10 °C. The temperature response time of the liquid crystals is important and should be considered to ensure accurate temperature measurements. The response time of the Hallcrest encapsulated chiral nematic liquid crystals was evaluated by many authors[20,22] and appears to be in the order of 1 to 4 ms.

The crystallizer and the jacket are cylindrical, but a Plexiglas lens was used to avoid the distortion of the images by the wall curvature. The light was provided by a LED fiber optic illuminator (REVOX, SLG-50s). The crystallizer was illuminated in a vertical plane by a sheet of light with a tichness of 2−3 mm, while the camera was positioned perpendicular to the illuminated plane.

2.2. Determination of 2-D Velocity, Temperature, and Initial Supersaturation Using the PIV/PIT Method. In this paper the PIT/PIV method is applied for the simultaneous measurement of the 2D profile of the temperature, initial supersaturation, and the velocity field in the crystallizer. This detailed information on the local process conditions is extremely important to control the product quality in batch seeded crystallization processes.[23] In practice it is assumed that the temperature is uniformly distributed, and it is measured in one point in the crystallizer. However the temperature and thus the supersaturation are not always uniformly distributed throughout the crystallizer. In this work a PIT method is applied for initial supersaturation measurements. 2-D velocity, temperature and supersaturation measurements are very important to determine the efficiency of the mixing, the seeding point, or the place where primary nucleation occurs.

The liquid crystals added to the fluid follow the flow dynamics if the particles are sufficiently small. The Stokes number (St) provides a measure of the particles ability to track the flow field, and it depends on the flow geometry and the presence of significant accelerations or decelerations. The Stokes number is defined as the ratio of the characteristic time of a particle to a characteristic time of the flow. For acceptable tracing accuracy, the particle response time should be faster than the smallest time scale of the flow. Smaller Stokes numbers represent better tracing accuracy. For St between 0.1 and 1, particles detach from a flow especially where the flow decelerates abruptly. In the experiments conducted in this work $St \ll 0.1$, and it is assumed that particles follow the fluid streamlines accurately. The instantaneous fields of the vector velocity are obtained by measuring the displacement of numerous fine liquid crystals that follow the movement of the liquid.

The acquisition speed of the camera could be varied from 1 to 285 frames per second, and a total of 2270 frames were recorded for each experiment. The size of the images is 960 × 1710 pixels, and the pixel size is 87 μm. The average velocity fields were obtained by averaging 100 to 400 instantaneous velocities fields. In each point along the radius, r, and the height, h, of the crystallizer a local resultant velocity, $w(r,h)$, can be calculated from the velocity components along the horizontal and vertical directions

$$w(r, h) = \sqrt{v_r^2 + v_h^2} \tag{1}$$

From the time average velocity fields a volume mean velocity can be calculated, which allows for a quicker comparison between different operations. In the case of the airlift crystallizer, mean velocities can be calculated in the riser and in the down-comer for different air flows. The mean velocities averaged along the riser (z_R) and down-comer (z_D) can be calculated as

$$W_R = \frac{\int_{h1}^{H} \left(\int_0^{R_R} w(r, h) \cdot 2\pi r \cdot dr \right) \cdot dh}{\pi \cdot R_R^2 \cdot (H - h1)} \tag{2}$$

$$W_D = \frac{\int_{h1}^{H} \left(\int_{R_R}^{R_D} w(r, h) \cdot 2\pi r \cdot dr \right) \cdot dh}{\pi \cdot (R_D^2 - R_R^2) \cdot (H - h1)} \tag{3}$$

where R_R is the riser radius, R_D is the down-comer radius, H is the height of the analyzed zone of the crystallizer, $h1$ is the height were the riser starts, r and h are the current radius and height, respectively, and w is the local resultant velocity.

Two-dimensional temperature fields can be obtained by using the PIT method. When the liquid crystals are illuminated with white light, the color of the light reflected changes as a function of the temperature from colorless, at low temperature, to red, green, blue, and again colorless for successively higher temperatures. A few examples of the color change with the temperature are shown in Figure 3. A solution saturated at 26 °C was heated up at 31 °C and then slowly cooled down to 24 °C, checking that the solution was still clear. After reaching a constant uniform temperature in the entire vessel, images were taken at temperature intervals of 0.5 °C. The concentration of the solution remained constant during the experiments because no crystal nucleation took place due to the fact that the maximum undercooling was within the metastable limit of the compound. For each image a mean hue value was calculated, and a calibration curve for the temperature as a function of hue value was determined, as in eq 4

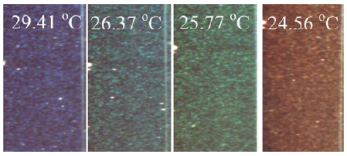

Figure 3. Examples of images used for calibration.

$$T = 3.57 \cdot 10^{-4} e^{(13.23H)} + 3.081H + 24.15 \tag{4}$$

where T is the temperature, in °C, and H is the hue value.

The goodness of the fit characterized by the R-square, which represents the sum of the square of the differences between the measured and the predicted values, had a value of 0.9974. The calibration curve was used to calculate the 2-D temperature profiles during the experiments where the temperature varied between 24 and 31 °C. The 2-D relative supersaturation profiles can be calculated from the temperature profiles if the initial concentration of the solution is known, assuming a constant and uniform concentration throughout the vessel. This assumption is valid if the evaporation of the solvent is negligible and if no nucleation takes place during the experiment.

The relative supersaturation, in %, is calculated as

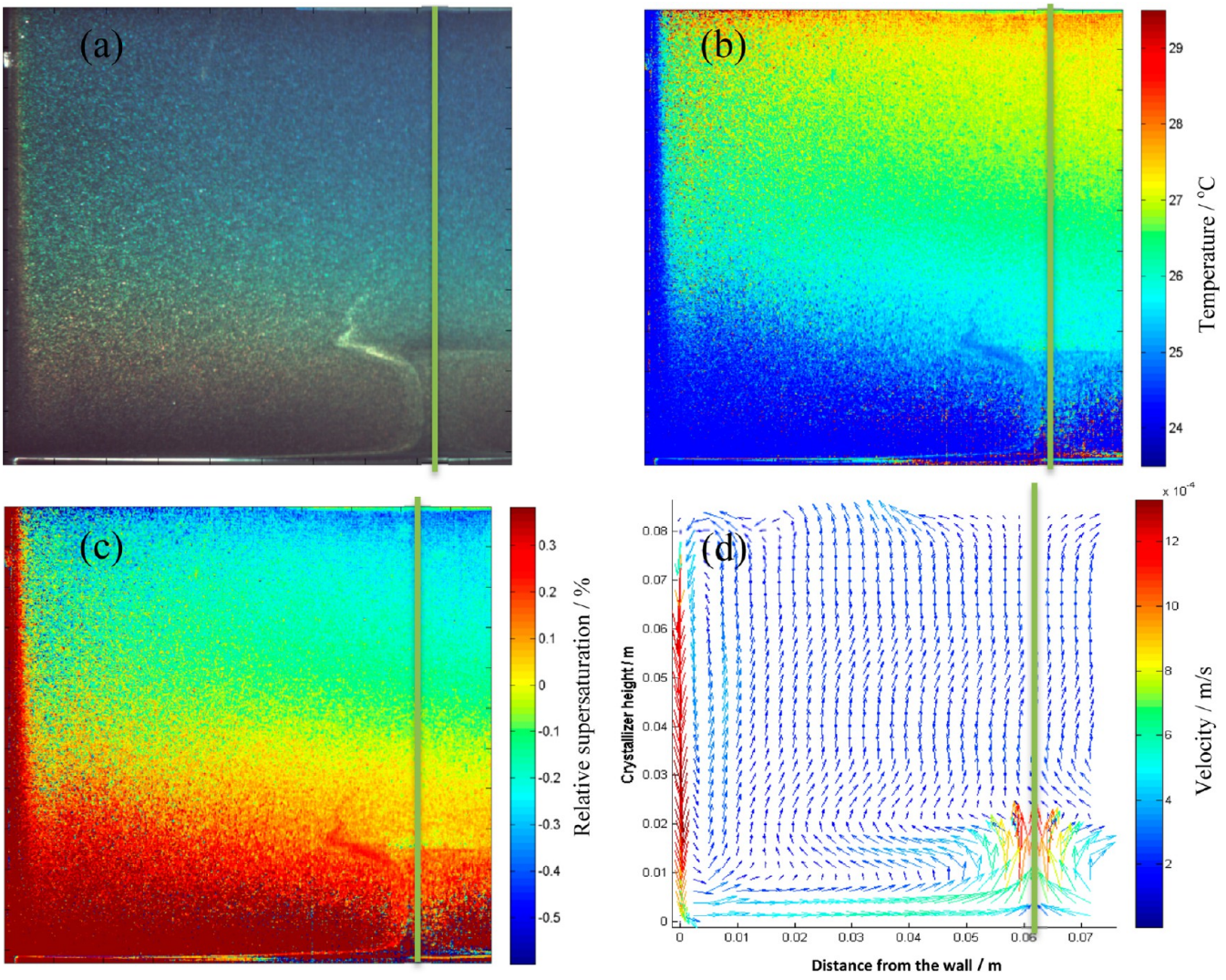

Figure 4. Cooling experiment by natural convection: (a) captured image, (b) temperature field, °C, (c) relative supersaturation field, %, (d) average velocity field, m/s. The green line from each picture marks the center of the vessel.

$$\sigma = \frac{c - c_s}{c_s} \cdot 100 \tag{5}$$

where c is the concentration of the solution, and c_s is the saturation concentration. According to Daudey et al.,[24] the saturation concentration for ammonium sulfate can be calculated using the following formula

$$C_s = 0.41179 + 9.121 \cdot 10^{-4} T \tag{6}$$

where T is the local temperature in °C.

2.3. Method Validation - Simultaneous 2-D Flow, Temperature, and Supersaturation Measurements. To demonstrate the feasibility of the simultaneously 2-D measurements of velocity, temperature, and supersaturation a cooling experiment was conducted. The jacketed vessel described in section 2 was filled with a solution of ammonium sulfate−water saturated at 26 °C. Two droplets of liquid crystal slurry were added into the solution.

The vessel was illuminated in a vertical plane by a sheet of light with a thickness of 2−3 mm, while the camera was positioned perpendicular to the illuminated plane.

The solution was heated to 31 °C, and a cooling experiment was performed. No mixing was applied to the vessel in order to clearly see the supersaturation gradients. The temperature of the cooling agent was fixed at 23 °C to obtain a maximum undercooling of 3 °C, well within the metastable limit for this compound and thus avoiding primary nucleation.

Figure 4a represents the image captured 10 min after the start of the cooling. The left-hand side edge is the wall between the jacket and the vessel, and the green vertical line is the central axis of the vessel. Figure 4b represents the calculated 2-D temperature profile. Figure 4c represents the relative supersaturation profile, and Figure 4d represents the average velocity profile. In the calculations it is assumed that the solute concentration remains equal to the initial concentration (no crystallization or evaporation) and is uniformly distributed over the vessel. The solution close to the jacket wall started to cool down, and the cooler (more dense) solution is accumulating at the bottom of the vessel. It can be observed that there are large temperature and supersaturation gradients along the vessel.

The mean supersaturation in Figure 4c is 0.02%, but a wide variation of the supersaturation can be observed along the vessel. At the top of the vessel the solution is undersaturated, and at the bottom of the vessel the solution is supersaturated. This wide variation of the supersaturation occurs because the vessel is cooled down and no stirring is applied. Figure 4d

dx.doi.org/10.1021/ie4006723 | Ind. Eng. Chem. Res. 2013, 52, 12212−12222

shows a high downward velocity close to the wall, as the cooler solution flows at the bottom of the vessel, and a high upward velocity in the center of the vessel, as the warmer, less dense solution flows at the top of the vessel. This experiment shows that the used method is feasible to measure simultaneously the 2-D velocity, temperature and supersaturation fields. It should be noted that the supersaturation field can only be determined in the absence of crystallization or evaporation. The temperature resolution of the liquid crystal is 0.1 °C, and the resolution of the relative supersaturation is in 10^{-4}%.

3. RESULTS

3.1. 2-D Flow Measurements in the Airlift Crystallizer.

A saturated ammonium sulfate−water solution was prepared at 20 °C in a separate vessel, poured in the airlift crystallizer, and heated to 25 °C in order to have clear solution. The air injected in the crystallizer has a temperature of approximately 23 °C (room temperature). The air flows used in the experiments are 10, 50, 100, and 300 L/h. These air flow rates correspond to overall superficial air velocities based on the total cross-sectional area of 0.3, 1.2, 2.3, and 7 mm/s.

In Figure 5, a few captured images are depicted at different air flow rates. It can be observed that the air holdup increases with the increase of the air flow rate and that the bubble size distribution varies with the air flow rate. For air flows smaller than 100 L/h the 2 L crystallizer operates in regime I and for higher air flow rates the operation regime becomes II. The experiments conducted in regime III, at air flow rates higher than 700 L/h, showed an increase in the gas holdup and a considerable decrease in the visibility. Extracting the velocity vectors in the presence of the bubbles can be done by removing the bubbles from the pictures using image preprocessing with a threshold that removes the white and high intensity pixels. However this preprocessing is meaningful only for air flow rates up to 300 L/h, when after the bubble removal the amount of information remaining is still high enough to obtain the velocity vectors. In Figure 5, it can be observed that the liquid has different colors in each image, due to different liquid temperature (between 25 and 31 °C).

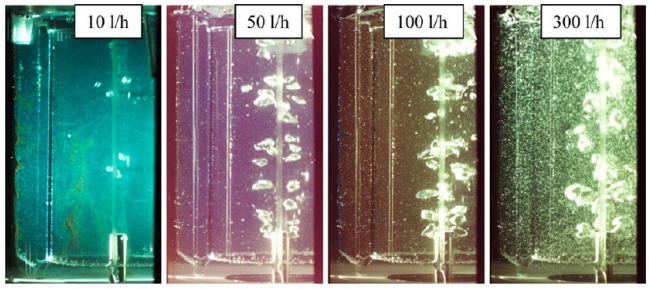

Figure 5. Snapshots of the visualization; experiments with 4 holes sparger, at different temperatures and 4 different air flow rates.

The acquisition speed of the camera was 285 frames per second. The average velocity field was obtained by averaging 400 instantaneous velocity fields. From the instantaneous flow fields it was observed that the turbulence increased with the air flow rate. If the flow rate is increased, then the bubbles are detached from the sparger with a higher frequency and velocity. If the velocity of the bubbles detached from the sparger is higher, then the difference between the liquid and bubble velocity is higher and vortexes are formed from the center to the internal wall of the riser.

Figure 6 gives the average result for the velocity field induced by the sparger with 4 holes for three different air flow rates: 50 L/h, 100 L/h, and 300 L/h air. Because of the averaging the overall flow is obtained and the instantaneous local resolution is lost. As expected the overall flow is upward in the riser and downward in the down-comer.

The mean velocity magnitude increases with the air flow rate as can be seen in Table 1. In order to test the influence of the number of holes in the sparger on the flow, experiments using a different sparger with 32 holes were conducted. The average velocity fields are shown in Figure 7.

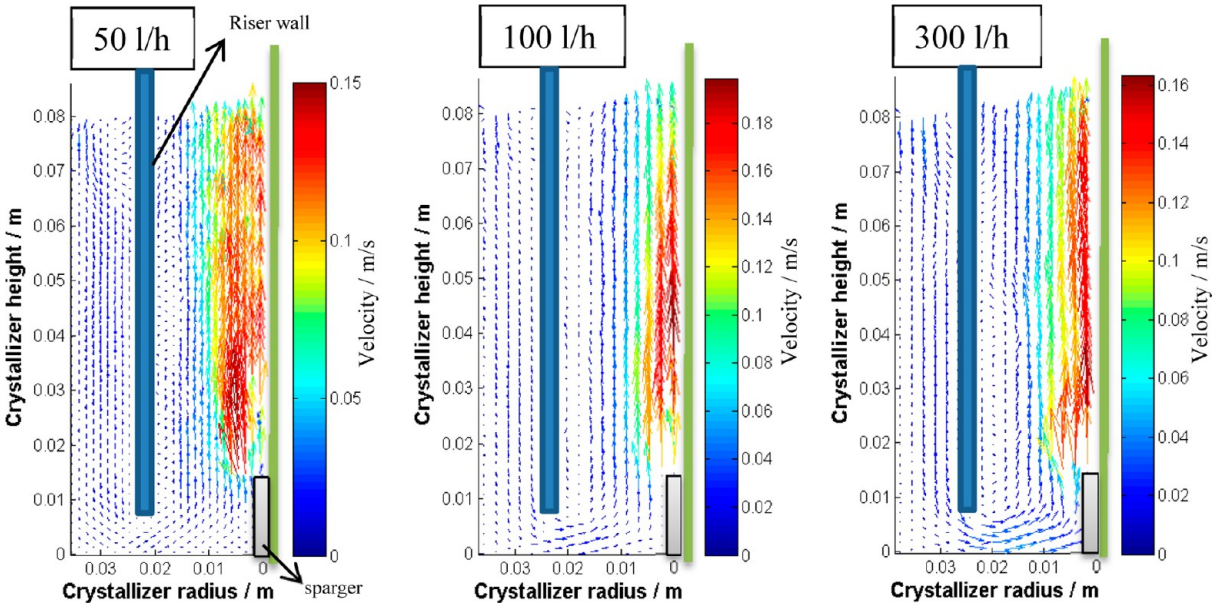

Figure 6. Average velocity fields obtained from experiments performed using a 4-hole sparger at three air flow rates. The green line from each picture marks the center of the vessel.

dx.doi.org/10.1021/ie4006723 | Ind. Eng. Chem. Res. 2013, 52, 12212−12222

Table 1. Mean Velocities in the Riser w_R and Downcomer w_D at Different Air Flow Rates and Different Number of Holes on the Sparger

measured property	sparger with 4 holes			sparger with 32 holes		
air flow rate, L/h	50	100	300	50	100	300
liquid mean velocity in the riser, cm/s	3.64	4.26	5.81	4.76	5.26	4.78
liquid mean velocity in the down-comer, cm/s	1.50	1.51	1.47	1.56	1.28	1.13

The velocity of the mixture induced by the 32 holes sparger is slightly increased in the riser compared to the velocity induced by the one with 4 holes for the same air flow rates, see Table 1. This is caused by the fact that the bubbles leave the sparger at a lower linear velocity as the gas flow is divided over more holes. This results in a larger bubble size and in a smaller bubble detachment velocity. Because the bubbles initial velocity is smaller, the vortexes induced in the liquid are less strong. At an air injection rate of 100 L/h, the velocity in the riser is larger in case of 32 holes, whereas it is smaller in the downcomer. This suggests that under these conditions the gas holdup is different and that it might give the differences in the velocities.

The experiments were repeated, and the average velocity fields were reproducible. The error in the values of the velocity is expected to increase with the air flow rate due to a wider bubble size distribution. If the air bubbles and the liquid crystals are comparable in size, then they are difficult to distinguish and they induce errors in the measurements.

For 300 L/h the operation regime is II, and many small bubbles are entrained in the down-comer as can be observed in Figure 5. Due to the increased amount of small bubbles in the down-comer the liquid velocity is decreased as the driving force for the circulation flow decreases due to the lower density differences between riser and down-comer. An easy solution for the entrainment of bubbles in the down-comer and for maintaining high liquid velocities is the use of a disengagement zone on top of the down comer as was shown in a previous study.[5]

As can be seen in Figures 6 and 7, the flow is not uniformly distributed over the riser part of the airlift. The bubble flow is concentrated in the central part of the riser despite the fact that the gas flow is directed outward. There is definitely room for improvement of the sparger geometry, and the PIV method is a valuable tool to optimize the sparger design. The flow can be improved by using a sparger which can distribute the bubbles more uniformly at the bottom of the riser, like a ring or star shape sparger.

3.2. 2-D Temperature Measurements in the Airlift Crystallizer. In order to determine the minimum air flow rate that can induce enough mixing to ensure minimum temperature and supersaturation gradients along the crystallizer, experiments were conducted in which 2-D temperature profiles were measured.

After the calibration, cooling and heating experiments were performed with a temperature change rate of 1.7 °C/min and different air flow rates. This cooling rate is higher than the ones used in crystallization experiments and was chosen to highlight the temperature gradients. In Figure 8, the result of a heating experiment is depicted. The air flow rate is fixed at 10 L/h. At the start of the experiment both the crystallizer and the jacket temperature are fixed at 23 °C, and during the experiment the jacket temperature is increasing with a constant rate of 1.7 °C/min. Figure 8a represents one of the images captured a few minutes after the start of the experiment, and Figure 8b shows the 2D temperature profile. It can be observed that there are big temperature gradients both along the riser and down-comer and that the mixing is not good enough.

In Figure 9 a second heating experiment is depicted at an air flow rate of 50 L/h. Figure 9b shows the 2D temperature profile. It can be observed that the temperature gradients are decreased both along the riser and down-comer and that the mixing is improved compared to the first experiment. However, at the external down-comer wall, which separate the down-comer from the jacket, high temperature gradients of 4 °C still exist. For an air flow rate higher that 100 L/h the mixing is very

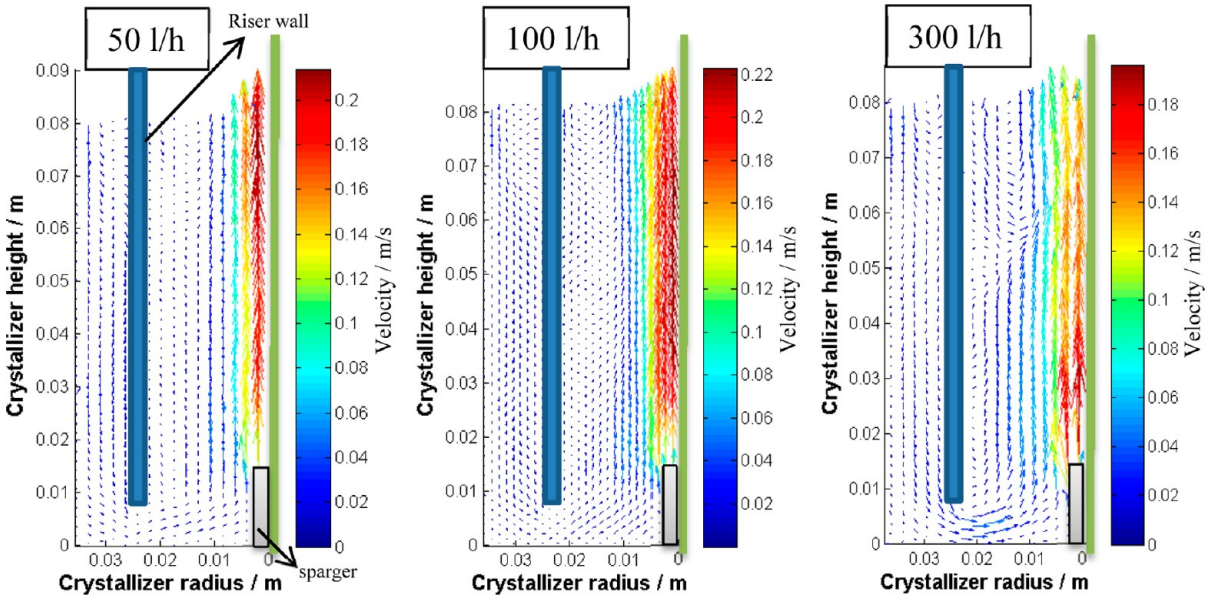

Figure 7. Average velocity fields obtained from experiments performed using a sparger with 32 holes at three air flow rates. The green line from each picture marks the center of the vessel.

dx.doi.org/10.1021/ie4006723 | Ind. Eng. Chem. Res. 2013, 52, 12212−12222

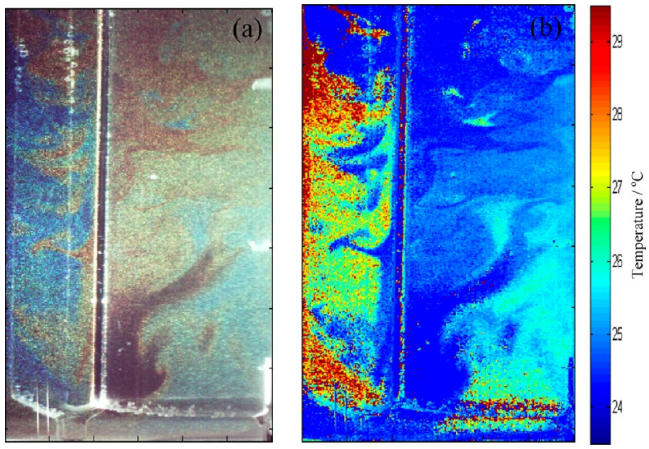

Figure 8. Temperature profile of an experiment with an air flow rate of 10 L/h (a − captured image, b − temperature field).

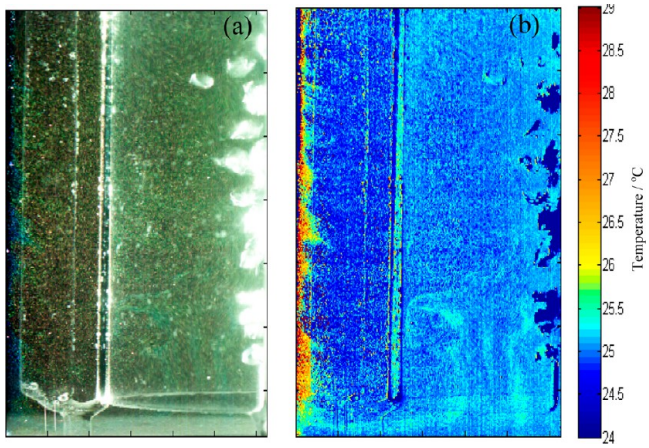

Figure 9. Temperature profile of an experiment with an air flow rate of 50 L/h (a − captured image, b − temperature field).

good, and there are very low temperature gradients inside the crystallizer and along the internal down-comer wall.

Supersaturation fields were not plotted because the solution was slightly undersaturated to ensure that no crystallization takes place. However, by analyzing the temperature gradients it is obvious that for air flow rates higher that 100 L/h the supersaturation gradients will be very low as well.

3.3. Crystal Suspension Tests and Criteria. In addition to the velocity measurements, crystal suspension tests were conducted to check the capability of the airlift crystallizer to suspend the crystals. Two types of tests were performed. The first test aimed at checking the uniformity of the suspension at a constant gas flow by visual inspection. The second test aimed at checking the resuspension of the crystals after settling at the bottom by switching off the gas flow temporarily.

To study the suspension behavior in the airlift crystallizer at different air flow rates, the crystal settling behavior was examined at increasing crystal loads of very large crystals (1.5 mm). The settling was examined by visual inspection, and the crystal size was chosen to create a worst case scenario for the settling. The test showed that for an air flow rate of 100 L/h a crystal holdup of up to 3 wt % was totally suspended with no indication of accumulation of crystals at the bottom. For an air flow rate of 200 L/h a crystal holdup of up to 6 wt % was totally suspended, while for an air flow rate of 300 L/h no sign of settling was observed up to 10 wt %. In addition when the air flow was interrupted, causing settling of all the crystals at the bottom of the crystallizer, a restart of the air flow induced a very fast resuspension of the crystals from the bottom. This ensures the stability of the crystallizer during operation in case of any perturbation of the air pressure or flow rate.

Mersmann et al.[25] introduced two criteria for crystal suspensions in stirred vessels which allows for the calculation of the minimal power input required to sustain the crystal suspension of a certain quality throughout the crystallization process. The two criteria are the mean specific power input ε_{BL} necessary for off-bottom lifting of the particles and the mean specific power input ε_{AS} necessary for avoidance of particle settling. ε_{BL} and ε_{AS} can be calculated as described in Appendix A. ε_{BL} is dominant in small scale vessels, but it cannot be calculated for an airlift crystallizer as it is a function not only of the suspension properties and crystallizer geometry but also a function of the impeller diameter. ε_{AS} is the decisive parameter in large vessels and can be calculated in an airlift crystallizer as it is a function only of the suspension properties. The fact that the deposition of particles at the bottom of the vessel is prevented does not guarantee that the particle settling is insignificant and vice versa. The mean specific power input that is required to fulfill both criteria may be conservatively assumed to be the sum of the ε_{AS} and ε_{BL}. Kalbasenka[26] showed that in a 75 L draft tube crystallizer the ε_{BL} has equal importance as ε_{AS} (ε_{AS} = 1.15 ε_{BL}), and in a 1100 L draft tube baffle crystallizer ε_{AS} is the dominant criterion (ε_{AS} = 3.2 ε_{BL}).

In airlift crystallizers the specific power input P, defined as the power input given by the gas per unit of liquid volume, is due to gas isothermal expansion along the riser height[27]

$$P = \frac{Q_g RT}{V_L} \ln\left(1 + \left(\frac{\rho L g Z}{P_a}\right)\right) \tag{7}$$

where Q_g is the molar gas flow rate, R is the ideal gas constant, T is the gas temperature, V_L is the liquid volume, ρ_L is the liquid density, g is the gravitational acceleration, Z is the fluid height, and P_a is the pressure at top of the liquid.

In the experiments conducted in the 2 L airlift crystallizer the maximum solid holdup that can be maintained uniformly in suspension and can be lifted from the bottom of the crystallizer was measured for three air flow rates. The mean specific power input ε_{AS} necessary for avoidance of particle settling was calculated for these three air flows together with the specific power input introduced by the air.

Once the total power input needed was obtained from the experiments and the power input necessary for avoidance of particle settling was calculated, the power input necessary for off-bottom lifting of the particles can be estimated by subtracting one from the other as can be seen in eq 8.

$$\varepsilon_{BL} = \varepsilon_{Total} - \varepsilon_{AS} \tag{8}$$

Figure 10 shows the air flow rate dependence of the measured total power input, the estimated power input necessary for avoidance of particle settling, and the subtracted power input necessary for off-bottom lifting of the particles. As expected, in the small vessel with crystals of 1.5 mm, the off-bottom lifting is the dominant criterion (ε_{BL} = 2.4 ε_{AS}).

The avoidance of settling criterion could be used for the calculation of the air flow rate which is necessary to sustain the crystal suspension of a certain quality in airlift crystallizers. As in a 2 L scale airlift the off-bottom lifting criterion is almost

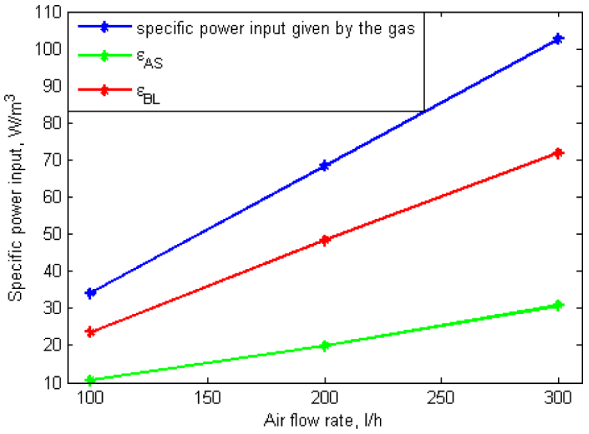

Figure 10. The specific power input given by the gas and avoidance of settling and off-bottom lifting criteria function of the gas flow rate.

three times higher than the avoidance of settling criterion and the importance of the off-bottom lifting criterion is decreasing with the scale, a total mean specific power input equal to five times the avoidance of settling criterion should be sufficient to ensure the desired quality of the crystal suspension at any scale of the crystallizer at least up to the studied crystal sizes and concentrations, i.e. 1.5 mm and 10 wt %.

3.4. Considerations on the Crystal Growth Dynamics.

Crystal growth involves the incorporation of solute molecules into the crystal lattice of already existing crystals. It requires mass transfer of the solute molecules from the bulk of the solution to the crystal surface followed by surface diffusion on the crystal surface and incorporation in a kink location of the growing crystals. To ensure high enough mass transfer rates from the bulk to the crystal phase, turbulent conditions are recommended.[28] To investigate whether such conditions are met in the airlift crystallizer, the degree of surface integration or diffusion limited growth has been quantitatively determined through the effectiveness factors of crystal growth as proposed by Garside.[29] The integration effectiveness factor and the diffusion effectiveness factor were calculated as described in Appendix B. The overall crystal growth rate values are determined from two seeded experiments executed in an 18 L airlift crystallizer.[5] The seeds, which had the mean size of 125 μm, were grown in a period of 200 min to a size of 390 μm in the first experiment and to a size of 580 μm in the second one with a smaller seed load. The properties of the ammonium sulfate solution and crystals used for the calculations are given in Table 2. The surface integration rate coefficient varies with the supersaturation, temperature, and crystal size, and its value can vary in different experiments. For the purpose of the effectiveness factors calculation the surface integration rate coefficient was varied between $2.5\cdot10^{-5}$ and $7.7\cdot10^{-5}$ m^4/mol/s, values estimated from multiple experiments by Neumann[30] and Kalbasenka.[26] The Damköhler number and the effectiveness factors are calculated as a function of the surface integration.

Table 2. Ammonium Sulfate Solution and Crystals Properties

property	value
diffusion coefficient, D	$1.1\cdot10^{-9}$ [m/s][31]
gravitational acceleration, g	9.81 [m/s^2]
solid density, ρ_S	1769 [kg/m^3][31]
liquid density, ρ_L	1250 [kg/m^3][31]
liquid viscosity, η_L	10^{-3} [kg/m/s][31]
mean crystal size, L	390; 580 [μm][5]
mean liquid velocity, w	1.5; 5 [cm/s]
order of the integration, r	2[26,30]
growth rate, R_G	$2.9\cdot10^{-4}$; $5.1\cdot10^{-4}$ [mol/m^2/s][5]
surface integration rate coefficient, k_r	$2.5\cdot10^{-5}$–$7.7\cdot10^{-5}$ [m^4/mol/s][26,30]

At very small values of the Damköhler number the integration effectiveness factor approaches unity and the diffusion effectiveness factor approaches zero representing a pure surface integration limited growth. At very large values of the Damköhler number the integration effectiveness factor approaches zero and the diffusion effectiveness factor approaches unity representing a pure diffusion limited growth.

In Figure 11 the variation of the surface integration and diffusion effectiveness factors with the surface integration coefficient are depicted. It can be observed that for a mean liquid velocity of 1.5 cm/s the growth is mainly limited by diffusion, especially when the crystals have larger sizes. For a mean liquid velocity of 5 cm/s and large crystals the diffusion limits the crystal growth. For small crystals the growth is surface integration limited.

The supersaturation, calculated with eq B6 in Appendix B, varies from 1.4 to 6.2 mol/m^3, equivalent to 0.2 to 0.8 °C undercooling. These values of the supersaturation are reasonable for ammonium sulfate–water system and comparable with the values of supersaturation measured and obtained from simulations by Kalbasenka.[26] The data presented in Figure 11 are approximate and are intended to provide information on the limitations on the crystal growth in an airlift crystallizer. An exact calculation of the effectiveness factors of crystal growth requires exact calculations of the k_d and k_r coefficients as functions of all the process variables (time, crystal size, supersaturation, temperature), and this requires further theoretical and experimental research. However, Figure 11 shows that if L increases, k_r increases as it is proportional with L^2, k_d decreases as it is proportional with $L^{-1/2}$, and Da number increases as it is proportional with $L^{5/2}$, making η_r to decrease. For a batch process the crystal growth is limited by surface integration at the beginning of the batch and mainly by diffusion at the end of the batch, especially for low circulation velocity and high product size. This behavior can be explained by the fact that the growth rate depends on the number of dislocations on the crystal. Therefore, it can be assumed that large crystals have so many dislocations that the integration of units does not prevent growth. On the other hand, it is precisely the integration reaction that can limit the growth of small crystals if these have only a few dislocations.[1]

This study shows that the crystal growth in an airlift crystallizer behaves comparable to that in a suspension stirred crystallizer and we found no evidence for mass transfer limitation of the growth of the crystals. The crystal growth is not always integration controlled, but this is not due to the limited agitation in the crystallizer. It has been shown in different studies[24,32] in impeller mixed crystallizer that for ammonium sulfate–water system the growth is diffusion controlled or both diffusion and integration controlled. Kitamura et al.[32] found that the growth process of large ammonium sulfate crystals is highly controlled by volume diffusion and that the effect of volume diffusion on other salts such as potassium sulfate is not as significant.

dx.doi.org/10.1021/ie4006723 | Ind. Eng. Chem. Res. 2013, 52, 12212–12222

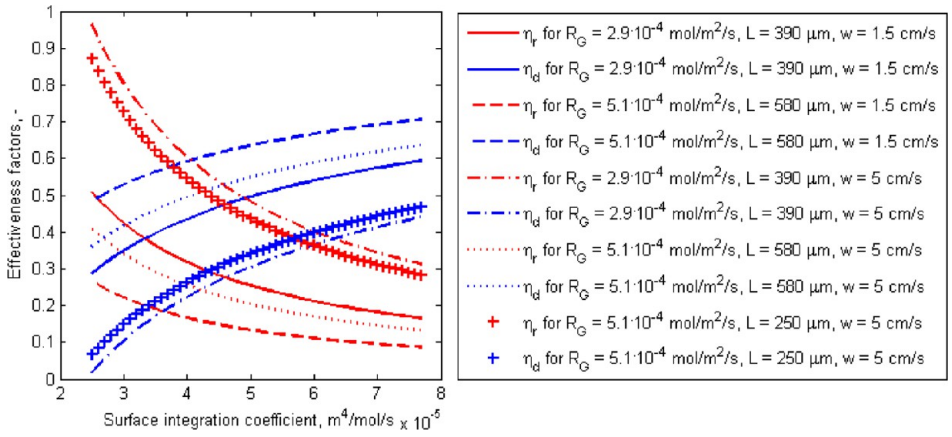

Figure 11. Effectiveness factors for crystal growth.

4. CONCLUSIONS

A combined PIV and PIT method was applied to visualize and measure simultaneously the velocity and temperature profiles in an airlift crystallizer. With this technique also the initial supersaturation profile in the crystallizer, before nucleation or seeding takes place, can be visualized in real-time. The method can be used to optimize the hydrodynamics in impeller, pump or air driven crystallizers by determining spots with high supersaturation, zones with bad mixing, and locations where primary nucleation takes place and thus can also be used to determine the optimal seeding point. It can be applied for characterization and optimization of lab scale crystallizers or for visualization of the initial supersaturation in important zones in bigger crystallizers.

The operation of an airlift crystallizer is not straightforward, and the control of the product quality requires an extensive knowledge of the flow and mixing conditions induced by the released air flow. Application of the PIT/PIV method allows the optimization of the process conditions to achieve uniform distributions of the supersaturation and crystal suspension. Experiments were performed in 2 L crystallizer, and the hydrodynamic behavior was studied for different air flow rates, sparger types and crystal holdup. The 2-D velocity and temperature gradients showed that the crystallizer has a good mixing with very small temperature gradients for air flow rates higher than 100 L/h (superficial air velocities higher than 2.3 mm/s) even for high temperature change rates. The suspension test showed that for an air flow rate of 300 L/h (superficial air velocities higher than 7 mm/s), the power input was sufficient to avoid the settling of the crystals and ensure the lifting of the solids from the bottom of the crystallizer for a crystal holdup of 10% with a mean size of 1.5 mm and to avoid mass transfer limitations of the growing crystals. The circulation velocity and the maximal suspended crystal holdup can be increased by the air flow rate. However the circulation velocity increase with the air flow rate was limited due to the increase of the gas holdup in the down-comer. In such cases a gas disengagement zone at the top of the crystallizer is recommended to maintain a flow regime I at higher air flow rates. Thus higher liquid circulation velocities can be obtained under these conditions, needed for the suspension of larger particles and higher solid holdups. High liquid velocities also ensure high mass transfer rates from the bulk to the crystal phase. To investigate whether such conditions are met in the airlift crystallizer, the degree of surface integration or diffusion limited growth has been quantitatively determined, and the study showed that the crystal growth in the airlift crystallizer behaves comparable to that in a stirred vessel.

It was found that even in a 2 L airlift crystallizer for air flows of 100 to 300 L/h (superficial air velocities of 2.3 to 7 mm/s) the mixing provided uniform temperature and therefore supersaturation profiles and an efficient suspension of 3 to 10 wt % crystal holdup of crystals of 1.5 mm.

APPENDIX A

Crystal−Suspension Criteria

Crystal−suspension criterion is a measure which allows calculating the minimal power input required to sustain the crystal suspension of a certain quality throughout the crystallization process. Mersmann et al.[25] introduced two crystal−suspension criteria, the mean specific power input ε_{BL} [W/kg] necessary for off-bottom lifting of the particles and the mean specific power input ε_{AS} [W/kg] necessary for avoidance of particle settling. ε_{BL} is dominant in small scale vessels, and ε_{AS} is the decisive parameter in large vessels. The mean specific power input that is required to fulfill both criteria is defined as

$$\varepsilon_{Total} = \varepsilon_{BL} + \varepsilon_{AS} \tag{A1}$$

The specific power inputs for impeller mixed crystallizers ε_{BL} and ε_{AS} are functions of the suspension properties, represented by the Archimedes number and the volumetric holdup, and the vessel geometry[25]

$$\varepsilon_{BL} = 200\, Ar^{0.5}[\varphi(1-\varphi)^n]^{3/4}\frac{\upsilon_L g(\rho_S - L)}{Z\rho_L}\left(\frac{D}{D_{imp}}\right)^{5/2} \tag{A2}$$

$$\varepsilon_{AS} = 0.4\, Ar^{1/8}[\varphi(1-\varphi)^n]\sqrt{L\left[\frac{g(\rho_S-\rho_L)}{\rho_L}\right]^3} \tag{A3}$$

where Ar is the Archimedes number, φ is the volumetric fraction of solids, n is an exponent which is a function of the Archimedes number, υ_L is the liquid kinematic viscosity, g is the gravitational acceleration, ρ_S is the density of the crystals, ρ_L is the density of the liquid, Z is the fluid height, D is the diameter of the draft tube, D_{imp} is the diameter of the impeller, and L is the crystal mean size.

The Archimedes number is a calculated function of the suspension properties

dx.doi.org/10.1021/ie4006723 | Ind. Eng. Chem. Res. 2013, 52, 12212−12222

$$Ar = \frac{L^3 g(\rho_S - \rho_L)}{\nu_L{}^2 \rho_L} \tag{A4}$$

The exponent n is calculated with the equations given below[26]

$$\begin{aligned}
n &= -0.1303 \ln Ar + 4.65 \quad \text{for } 10^0 < Ar < 10^1 \\
n &= -0.2389 \ln Ar + 4.90 \quad \text{for } 10^1 < Ar < 10^2 \\
n &= -0.3040 \ln Ar + 5.20 \quad \text{for } 10^2 < Ar < 10^3 \\
n &= -0.2041 \ln Ar + 4.51 \quad \text{for } 10^3 < Ar < 10^4 \\
n &= -0.0782 \ln Ar + 3.35 \quad \text{for } 10^4 < Ar < 10^5 \\
n &= -0.0217 \ln Ar + 2.70 \quad \text{for } 10^5 < Ar < 10^6 \\
n &= 2.40 \quad \text{for } Ar \geq 10^6
\end{aligned} \tag{A5}$$

APPENDIX B

Integration Limited Growth versus Diffusion Limited Growth

It is assumed that the diffusion and integration steps in crystal growth can be described by eqs B1 and B2, respectively

$$R_G = k_d(c_b - c_i) \tag{B1}$$

$$R_G = k_r(c_i - c*)^r \tag{B2}$$

where R_G is the growth rate, k_d is the mass transfer coefficient, c_b is the concentration in the bulk, c_i is the concentration in the solution at the crystal solution interface, k_r is the surface integration rate coefficient, c^* is the equilibrium concentration, and r is the order of the surface integration.

A quantitative measure of the degree of diffusion or surface integration control may be made through the effectiveness factors of crystal growth. A crystal growth rate effectiveness factor, η, is defined by Garside[29] as the ratio of the overall growth rate to the growth rate that would be obtained if diffusion offered negligible resistance and is given by

$$\eta_r = (1 - \eta_r Da)^r \tag{B3}$$

where η_r is the integration effectiveness factor, and Da is the Damköhler number for crystal growth which represents the ratio of the pseudo-first-order rate coefficient at the bulk conditions to the mass transfer coefficient, defined by

$$Da = \frac{k_r}{k_d}(c_b - c*)^{r-1} \tag{B4}$$

The diffusion effectiveness factor, η_d, is defined as

$$\eta_d = Da(1 - \eta_d)^r \tag{B5}$$

For $r = 1$ the sum of the two effectiveness factors is always 1, for $r = 2$ the sum of the two effectiveness factors varies between 0.75 and 1 as eqs B3 and B5 become order 2 polynomial functions of the Da number.

The supersaturation, $c_b - c^*$, is calculated from the growth rate relation B6 which is obtained by eliminating the unknown c_i between eqs B1 and B2.

$$R_G = k_r\left((c_b - c*) - \frac{R_G}{k_d}\right)^r \tag{B6}$$

The mass transfer coefficient is calculated based on a Frösling type correlation[33]

$$Sh = 2 + 0.44 Re^{1/2} Sc^{0.38} \tag{B7}$$

where Sh is the Sherwood number, Re is the Reynolds number, and Sc is the Schmidt number.

$$Sh = \frac{k_d L}{D} \tag{B8}$$

$$Re = \frac{\rho_L \bar{w} L}{\eta_L} \tag{B9}$$

$$Sc = \frac{\eta_L}{\rho_L D} \tag{B10}$$

where L is the mean crystal size, D is the diffusion coefficient, ρ_L is the liquid density, $\bar{w}$ is a resultant slip velocity, and η_L is the liquid viscosity.

It is considered that the resulting slip velocity, $\bar{w}$, consists of the contributions arising from three types of velocities:[33]

1) an effective velocity for neutral density particles, v_E, arising from velocity gradients in the neighborhood of the particle surface. This effective velocity is equal with the liquid velocity measured in the absence of the particles, as depicted in section 3.1.

2) the particle terminal velocity, v_t, which can be approximated to the settling velocity in still liquid. The settling velocity can be calculated as in the eqs B12 − B14.

3) an additional slip, v_s, arising from differences in inertia between the particles and the fluid. The value of v_s is lower than the settling velocity and for purposes of most calculation the v_s/v_t ratio of 0.2 may be used without considerable loss of accuracy.

The resultant slip velocity, $\bar{w}$, can be represented to a reasonable approximation by the rule of addition of orthogonal vectors

$$\bar{w} = (v_E^2 + v_t^2 + v_s^2)^{1/2} \tag{B11}$$

Both v_t and v_s are functions of density difference and are zero for neutral density particles.

$$v_t = \frac{1}{18} L^2 \frac{\rho_S - \rho_L}{\eta_L} g, \quad \text{for } Re_p < 1 \tag{B12}$$

$$v_t = 0.151 \frac{g^{0.71} L^{1.14}}{\eta_L^{0.43} \rho_L^{0.29}} (\rho_S - \rho_L)^{0.71}, \quad \text{for } 1 < Re_p < 10^3 \tag{B13}$$

$$v_t = 1.74 \sqrt{L \frac{\rho_S - \rho_L}{\rho_L} g}, \quad \text{for } 10^3 < Re_p < 10^5 \tag{B14}$$

where g is the gravitational acceleration, and Re_p is the particle Reynolds number and is defined as

$$Re_p = \frac{\rho_L v_t L}{\eta_L} \tag{B15}$$

AUTHOR INFORMATION

Corresponding Author

*E-mail: a.soare@tudelft.nl.

Notes

The authors declare no competing financial interest.

REFERENCES

(1) Mersmann, A. *Crystallisation Technology Handbook*; 1995; pp 215−325.

(2) Kramer, H. J. M.; Bermingham, S. K.; van Rosmalen, G. M. Design of Industrial Crystallisers for a Given Product Quality. *J. Cryst. Growth* **1999**, *198*, 729−737.

(3) Neumann, A. M.; Bermingham, S. K.; Kramer, H. J. M.; van Rosmalen, G. M. The Effect of the Impeller Speed on the Product Crystal Size Distribution a 22 Liter Draft Tube Crystallizer. *J. Cryst. Growth* **1999**, *198*, 723−728.

(4) Dorofeeva, M. I.; Koltsova, E. M.; Gordeev, L. S. Experimental Study and Mathematical Simulation of the Crystallization of Ammonium Sulfate in a Forced Circulation Crystallizer. *Theor. Found. Chem. Eng.* **2008**, *42* (1), 67−76.

(5) Soare, A.; Lakerveld, R.; van Royen, J.; Zocchi, G.; Stankiewicz, A. I.; Kramer, H. J. M. Minimization of Attrition and Breakage in an Airlift Crystallizer. *Ind. Eng. Chem. Res.* **2012**, *51* (33), 10895−10909.

(6) Joshi, J. B.; Ranade, V. V.; Gharat, S. D.; Lele, S. S. Sparged Loop Reactors. *Can. J. Chem. Eng.* **1990**, *68* (5), 705−741.

(7) Heijnen, J. J.; Hols, J.; vanderLans, R. G. J. M.; vanLeeuwen, H. L. J. M.; Mulder, A.; Weltevrede, R. A Simple Hydrodynamic Model for the Liquid Circulation Velocity in a Full-Scale Two- and Three-Phase Internal Airlift Reactor Operating in the Gas Recirculation Regime. *Chem. Eng. Sci.* **1997**, *52* (15), 2527−2540.

(8) Merchuk, J. C. Airlift Bioreactors: Review of Recent Advances. *Can. J. Chem. Eng.* **2003**, *81* (3−4), 324−337.

(9) Haut, B.; Halloin, V.; Cartage, T.; Cockx, A. Production of Sodium Bicarbonate in Industrial Bubble Columns. *Chem. Eng. Sci.* **2004**, *59* (22−23), 5687−5694.

(10) Saberi, A.; Goharrizi, A. S.; Ghader, S. Precipitation Kinetics of Sodium Bicarbonate in an Industrial Bubble Column Crystallizer. *Cryst. Res. Technol.* **2009**, *44* (2), 159−166.

(11) Rigopoulos, S.; Jones, A. Modeling of Semibatch Agglomerative Gas−Liquid Precipitation of Caco3 in a Bubble Column Reactor. *Ind. Eng. Chem. Res.* **2003**, *42* (25), 6567−6575.

(12) Adrian, R. J.; Westerweel, J. *Particle Image Velocimetry*; Cambridge University Press: Cambridge, New York, 2011.

(13) Ozawa, M.; Muller, U.; Kimura, I.; Takamori, T. Flow and Temperature-Measurement of Natural-Convection in a Hele-Shaw Cell Using a Thermosensitive Liquid-Crystal Tracer. *Exp. Fluids* **1992**, *12* (4−5), 213−222.

(14) Hiller, W. J.; Koch, S.; Kowalewski, T. A. 3-Dimensional Structures in Laminar Natural-Convection in a Cubic Enclosure. *Exp. Therm. Fluid Sci.* **1989**, *2* (1), 34−44.

(15) Hiller, W. J.; Koch, S.; Kowalewski, T. A.; Stella, F. Onset of Natural-Convection in a Cube. *Int. J. Heat Mass Transfer* **1993**, *36* (13), 3251−3263.

(16) Dabiri, D.; Gharib, M. The Effects of Forced Boundary Conditions on Flow within a Cubic Cavity Using Digital Particle Image Thermometry and Velocimetry (Dpitv). *Exp. Therm. Fluid Sci.* **1996**, *13* (4), 349−363.

(17) Li, H. M.; Xing, C. H.; Braun, M. J. Natural Convection in a Bottom-Heated Top-Cooled Cubic Cavity with a Baffle at the Median Height: Experiment and Model Validation. *Heat Mass Transfer* **2007**, *43* (9), 895−905.

(18) Kowalewski, T. A. Measurement of Temperature and Velocity Fields of Freezing Water Using Liquid Crystal Tracers. *Adv. Cold-Region Therm. Eng. Sci.* **1999**, *533*, 83−90.

(19) Kowalewski, T. A.; Rebow, M. Freezing of Water in a Differentially Heated Cubic Cavity. *Int. J. Comput. Fluid Dynamics* **1999**, *11* (3−4), 193−210.

(20) Park, H. G.; Dabiri, D.; Gharib, M. Digital Particle Image Velocimetry/Thermometry and Application to the Wake of a Heated Circular Cylinder. *Exp. Fluids* **2001**, *30* (3), 327−338.

(21) Park, H. G.; Gharib, M. Experimental Study of Heat Convection from Stationary and Oscillating Circular Cylinder in Cross Flow. *J. Heat Transfer* **2001**, *123* (1), 51−62.

(22) Gunther, A.; von Rohr, P. R. Influence of the Optical Configuration on Temperature Measurements with Fluid-Dispersed Tlcs. *Exp. Fluids* **2002**, *32* (5), 533−541.

(23) Kalbasenka, A. N.; Spierings, L. C. P.; Huesman, A. E. M.; Kramer, H. J. M. Application of Seeding as a Process Actuator in a Model Predictive Control Framework for Fed-Batch Crystallization of Ammonium Sulphate. *Part. Part. Syst. Charact.* **2007**, *24* (1), 40−48.

(24) Daudey, P. J. Crystallization of Ammonium Sulfate: Secondary Nucleation and Growth Kinetics in Suspension. Ph.D. Thesis, TU Delft, Delft, 1987.

(25) Mersmann, A.; Werner, F.; Maurer, S.; Bartosch, K. Theoretical Prediction of the Minimum Stirrer Speed in Mechanically Agitated Suspensions. *Chem. Eng. Process.* **1998**, *37* (6), 503−510.

(26) Kalbasenka, A. N. Model-Based Control of Industrial Batch Crystallizers: Experiments on Enhanced Controllability by Seeding Actuation. Ph.D. Thesis, TU Delft, Delft, 2009.

(27) Rengel, A.; Zoughaib, A.; Dron, D.; Clodic, D. Hydrodynamic Study of an Internal Airlift Reactor for Microalgae Culture. *Appl. Microbiol. Biotechnol.* **2012**, *93* (1), 117−129.

(28) Giulietti, M.; Seckler, M. M.; Derenzo, S.; Ré, M. I.; Cekinski, E. Industrial Crystallization and Precipitation from Solutions: State of the Technique. *Braz. J. Chem. Eng.* **2001**, *18*, 423−440.

(29) Garside, J. The Concept of Effectiveness Factors in Crystal Growth. *Chem. Eng. Sci.* **1971**, *26* (9), 1425−1431.

(30) Neumann, A. M. Characterizing Industrial Crystallizers of Different Scale and Type. Ph.D. Thesis, TU Delft, Delft, 2001.

(31) Westhoff, G. M. Design and Analysis of Suspension Crystallizers. Aspects of Crystallization Kinetics and Product Quality. Ph.D. Thesis, TU Delft, Delft, 2002.

(32) Kitamura, M.; Endo, H. Growth-Process of Ammonium-Sulfate Crystals Produced by Secondary Nucleation in Stirred-Tank Crystallizer. *J. Chem. Eng. Jpn.* **1991**, *24* (5), 593−599.

(33) Jancic, S. J.; Grootscholten, P. A. M. *Industrial Crystallization*; Delft University Press: Delft, 1984.